2015

Development of 3D Vision Testbed for Shape Memory Polymer Structure Applications

Kenneth Thompson
University of Central Florida

DEVELOPMENT OF 3D VISION TESTBED FOR SHAPE MEMORY POLYMER STRUCTURE APPLICATIONS

by

KENNETH THOMPSON
B.S. Arkansas State University, 2012

A thesis submitted in partial fulfillment of the requirements
for the degree of Master of Science
in the Department of Mechanical and Aerospace Engineering
in the College of Engineering and Computer Science
at the University of Central Florida
Orlando, Florida

Summer Term
2015

Major Professor:
Yunjun Xu

ABSTRACT

As applications for shape memory polymers (SMPs) become more advanced, it is necessary to have the ability to monitor both the actuation and thermal properties of structures made of such materials. In this paper, a method of using three stereo pairs of webcams and a single thermal camera is studied for the purposes of both tracking three dimensional motion of shape memory polymers, as well as the temperature of points of interest within the SMP structure. The method used includes a stereo camera calibration with integrated local minimum tracking algorithms to locate points of interest on the material and measure their temperature through interpolation techniques. The importance of the proposed method is that it allows a means to cost effectively monitor the surface temperature of a shape memory polymer structure without having to place intrusive sensors on the samples, which would limit the performance of the shape memory effect. The ability to monitor the surface temperatures of a SMP structure allows for more complex configurations to be created while increasing the performance and durability of the material. Additionally, as compared to the previous version, both the functionalities of the testbed and the user interface have been significantly improved.

ACKNOWLEDGMENTS

I would like to thank Dr. Yunjun Xu for pushing me to achieve more in my research as well has his constant help with any and all research tasks.

I would also like to thank the rest of the faculty and staff at University of Central Florida for helping me to expand my knowledge as well as helping me learn valuable engineering skills which I will carry with me forever.

I would also like to thank Dr. Jihua Gou and Dr. Kurt Lin for being on my thesis committee and advising me during this research.

I would also like to thank Lauren Henderson for her support and patience while I pursued my dream of higher education.

I would like to thank my labmates who helped me on this project, Dr. He Shen, August Mark, Pradens Pierre-Louis and Christian Garcia.

I would like to thank Dr. Fei Liang for helping me manufacture samples for testing and John Sparkman for helping 3D print components for the testbed and making samples for testing.

I would like to thank my friends and family for their constant support during my time in graduate school.

TABLE OF CONTENTS

LIST OF FIGURES

LIST OF TABLES

CHAPTER 1

INTRODUCTION

1.1 Stereo Vision

There has been much focus on using cameras for engineering applications since the 1980's. Most of the applications for stereo vision recently come from the robotics field for object detection [1], [2], [3]. The basis of most of these stereo vision reconstruction techniques is epipolar projection. In this method non-parallel image planes are projected into a parallel plane to resolve the 3D coordinates of an image point [4]. If these coordinates are found many manipulations can be used to discover other useful information, such as applying coordinate transformations and using perspective projection techniques to find new points of interest.

1.2 Calibration of Thermal Imaging Cameras

Since thermal imaging devices became available in the mid 1980's many people have been integrating them into their research. One difficulty that is experienced with thermal imaging cameras is that the traditional methods of RGB camera calibration [5], [6] involving checker-

board patterns are difficult to implement. To solve these issues many people have developed methods to generate thermal checkerboard grids to be used in the traditional calibration techniques [7],[8],[9]. These techniques are significantly limited by the fact that they are passive checkerboard heating techniques so the fidelity of the checkerboard decreases. A method of active checkerboard generation would greatly increase thermal camera calibration accuracy and allow thermal cameras to be used in more diverse applications.

1.3 Testbeds

The ability to test any engineering system in a controlled environment prior to application is very valuable, especially in the fields of dynamic modeling and control. To accomplish this, scaled down or more cost effective environments are created to allow the user to better control uncertainty when attempting to verify new physical or theoretical engineering concepts. Many people have designed and used testbeds in their research in this manner. In [10] the group developed a way to allow autonomous UAVs to attempt an in air refueling maneuver using a visual tracking algorithm. To test this algorithm it was not feasible to implement it on actual flying planes, so they decided to attach the refueling probe and drogue to the end of two 6 DOF robotic arms were used to simulate the motion of the aircraft attempting the refueling maneuver. In [11] a testbed was developed to allow for the testing of cooperative robotic hovercrafts over the internet. This testbed was designed with a certain amount of flexibility to allow for testing of many different control algorithms in one testbed. Another

testbed application was the use of vision and inertial sensing units as a method to monitor cubesat motion on a custom air bearing surface [12].

The testbed which is discussed in this thesis is a continuation of work which was conducted previously [13]. The main application of this testbed is to be able to monitor shape memory polymer composite structures during actuation to control their deflection. If precision control of these structures is possible many new applications for shape memory polymers could be implemented while increasing fundamental knowledge of shape memory polymer composite properties and capabilities.

1.4 Shape Memory Polymer

Shape memory polymers (SMPs) are a special type of smart material which posses the ability to retain a "memory" of a macroscopic "permanent" shape. These materials can then be manipulated and deformed into a "temporary" shape under special environmental conditions (heat,light or magnetic field) which will be retained until the stimulus is applied again and the material will revert back to the original stress free "permanent" shape. Shape memory polymers have several advantages to traditional shape memory alloy smart materials. The benefits to shape memory polymers compared to shape memory alloys is that SMPs are easier to manufacture,require lower activation temperatures, higher possible recovery strains, low cost and ease of material processing [14]. For these reasons, many researchers and engineers have recently began to conduct research into the use of SMP in structural applications.

Shape memory polymers are also capable of being actuated via different stimuli such as light [15], electromagnetic field [16], ambient heating [14][17] and electrical resistive heating [18]. With these clear benefits researchers have began to apply these SMPs to various fields of research. In the biomedical field people have used SMP as smart sutures [19], smart stents [20] and smart drug delivery systems [21]. Another key area of interest for shape memory polymers is in aerospace engineering summarized in [22] including use in hinges [23], deployable structures [24] [25] [26] and morphing wings [27] [28]. For all of these applications the ability to monitor the actuation temperature during design of the structures or devices is critical for their successful implementation. A method of monitoring temperature, actuation voltage, current and deflection could allow these preliminary areas of research to greatly improve their accuracy and efficiency during actuation.

1.5 Thesis Outline

Chapter two consists of the layout and implementation of the vision system within the testbed. It includes the geometrical constraints placed on the testbed, individual and stereo camera calibration techniques for both webcams and the thermal imager and correlation between the camera coordinate systems to locate pixel locations in each camera frame. The techniques discussed in this chapter can be directly applied to the testbed to locate tracked points in space and determine their temperature using the correlation process.

Chapter three consists of the design and implementation of the electrical system of the

testbed. It includes the electrical constraints for the testbed, breadboarding prototypes of the electrical system and the design of a printed circuit board for implementation in the final testbed. This chapter contains information about the electrical measurements and power distribution capabilities of the testbed and methods to increase the stability of the electrical system through printed circuit board fabrication.

Chapter four consists of the design and implementation of the graphical user interface for the testbed. The chapter contains information on the constraints for the GUI design and implementation.

Chapter five discusses the improvements in the current version of the testbed compared to the previous work. It also discusses two applications for the testbed which are thermal modeling of shape memory polymer composites and tracking and correlation of shape memory polymer structures. These are the two primary applications for this research in our laboratory.

Chapter six discusses the conclusions and future work which could be inspired by this work.

1.6 Contribution of Thesis

The contributions of this research are as follows, the two step correlation methods discussed allow for us to directly compute the temperature on any point of interest on the surface of a shape memory polymer structure. This research could benefit many applications in which spatial temperature information is required.

CHAPTER 2

VISION SYSTEM FOR MONITORING SHAPE MEMORY POLYMER STRUCTURES

2.1 Vision System Layout

2.1.1 Camera Configuration

The motivation of the camera orientation chosen was driven by the need to have the capability to simultaneously monitor geometry and temperature information of a structure from all sides. To accomplish this a layout of three stereo pairs was selected with an equidistant angle of 120° between the RGB vision cameras with the infrared thermal camera centered over the stage of the test bed. This orientation can be seen in Figure 2.1.

This configuration was selected because it was the most optimal configuration for surface deformation measurement on all sides of structure and as thermal cameras can be expensive the ability to see most of the surface with a single camera greatly reduced the cost of the vision system.

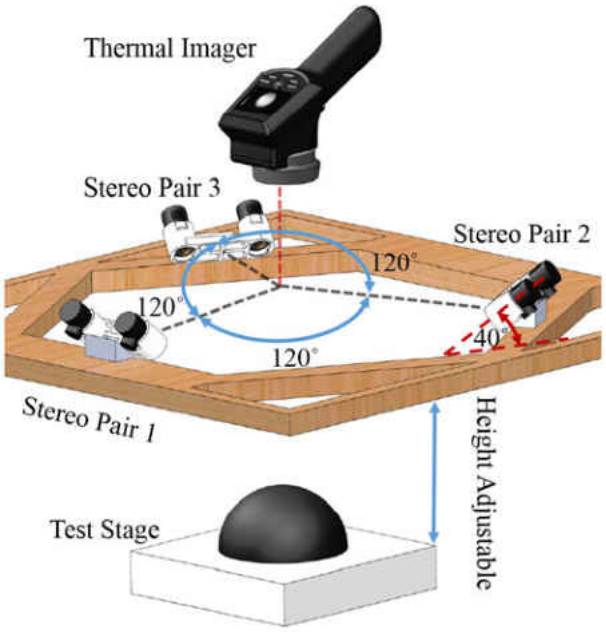

Figure 2.1: Layout of stereo pairs relative to the thermal camera with respect to the test bed stage.[29]

2.1.2 Four Camera Stereo Experiment

As with any stereo vision application the distance between the cameras in the stereo pair greatly affects both the accuracy and consistency of the distance measured by the pair. For our application we required the ability to consistently and accurately measure point locations to within one millimeter. To determine the distance separating the stereo pair we devised an experiment which would allow us to compare several distances at one time and select the best configuration for our needs. We set 4 identical cameras at distances 30 mm apart then used the Caltech Calibration toolbox [30] [6] to conduct a stereo calibration for each pair of cameras. With these calibration results we were able to select pixel locations of known

(measured) points of interest on a checker board patterned box with the box both parallel and at a 15° to the cameras and calculate the locations of these points in space relative to the coordinates of the left camera in the stereo pair. A summary of the results from this experiment can be seen in Table 2.1 below as well as the orientation of the checkerboard boxes which can be seen in Figure 2.2.

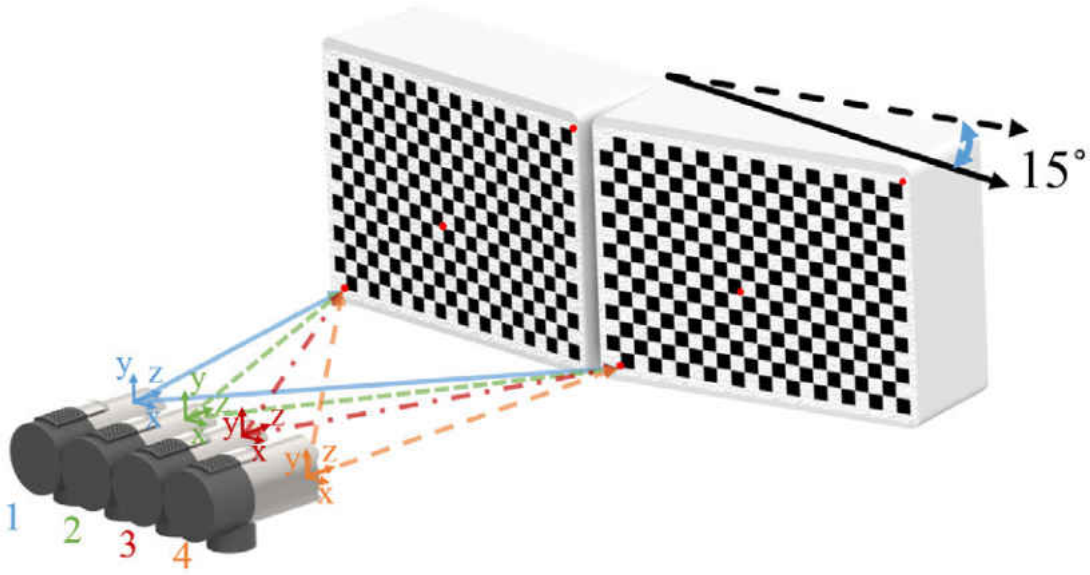

Figure 2.2: Four Camera stereo vision optimal placement experiment where 3 points are evaluated across the checkerboard pattern to test for accuracy and consistency in measurement data. The z distance between the cameras and the parallel board was 215mm for all points and 430mm, 480mm, 495mm.

Table 2.1: Four Camera Stereo Distance Results

	Parallel Configuration			15 ° Configuration		
	1-2 Pair	1-3 Pair	1-4 Pair	1-2 Pair	1-3 Pair	1-4 Pair
Point1						
x (mm)	-28.80	-28.77	-30.05	-0.73	-0.66	-0.69
y (mm)	60.55	60.34	63.28	58.39	52.40	52.82
z (mm)	205.25	205.12	214.10	473.57	423.60	431.01
Point2						
x (mm)	33.21	33.69	33.48	53.78	48.91	49.84
y (mm)	11.35	11.65	11.19	-0.27	-0.18	-0.63
z (mm)	215.21	218.37	216.92	518.82	471.81	480.69
Point3						
x (mm)	95.67	94.81	98.705	100.16	97.09	101.04
y (mm)	-29.71	-30.34	-31.16	-42.60	-40.45	-43.15
z (mm)	208.92	207.02	215.16	487.41	472.69	494.27

This experiment is designed to test the z-direction accuracy of the stereo pair as this is the direction in which large errors would cause inaccuracies in measurement of the surface geometry. The parallel board configuration was designed to test the consistency of the z-direction measurement by measuring different points that are located on the same plane a known distance away in the z direction which was 215 mm. It can be seen that both the 1-2 and 1-3 camera pairs at center to center distance of 30 and 60 mm respectively, showed very inconsistent measurements and were only to come near the correct measurement in 1 of the points each. The 1-4 camera pair at 90 mm center to center distance was able to get with 1mm on two of the three measurements and within 2 mm on the third which is within the desired tolerances of the system. The angled plane portion of the experiment was designed to test the accuracy of the system by attempting to locate the z-direction distance of various known distances for the 3 points being 430mm, 480mm, and 495mm respectively. Once again the 90mm center to center distance stereo pair performed within the desired accuracy tolerances and was thus selected as the distance that would be used in the final test bed vision system.

2.2 Camera Calibration

2.2.1 Webcam Calibration

The calibration method used to calibrate the RGB webcams was the very well documented checkerboard grid method using the Caltech Calibration toolbox[6][30]. This method relies on taking a series of images of a checkerboard grid of a known size in which each intersection point is recorded and used to determine the intrinsic parameters of the webcam. For the stereo vision application we do not need to find the extrinsic (position) parameters of the cameras as all of the calculations conducted are relative to the camera coordinate system not the physical position of the camera in the test bed.

2.2.2 Thermal Imager Calibration

In order to implement the correlation between the thermal and RGB webcams a method of calibrating the thermal camera using the Caltech toolbox is needed, which led to the development of our smart thermal grid system which would provide a thermal checkerboard pattern for calibration. Traditionally a thermal checkerboard pattern had been achieved via several methods, using a hairdryer to heat a checkerboard circuit [9] or metal wire grid [8], or placing a thermal mask over a hot plate [7]. Though these methods work initially they do not provide a consistent thermal grid pattern as with time the heat in the material will

dissipate leading to inconsistencies in grid edges as time progresses. To solve this issue we designed a self-regulating thermal grid which is capable of maintaining a constant temperature differential through a thermal wire grid overlaid on a traditional checkerboard to allow for simultaneous calibration of thermal and RGB webcams. The schematic for the system can be seen below in figure 2.3.

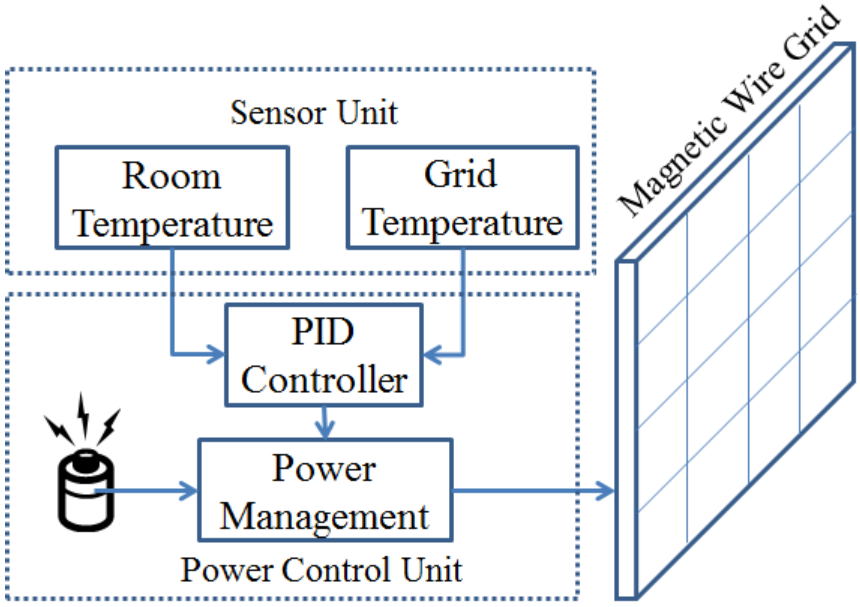

Figure 2.3: Thermal Camera Calibration tool schematic[29]

The calibration tool is composed of three main components, the sensor unit which is used to capture the ambient temperature and the wire grid temperature, the power control unit which uses an Arduino Uno board to regulate the voltage to the wire grid via a PID controller to control the temperature of the grid to the desired differential and the final component is the magnetic wire grid which consists of a single insulated wire that is woven into a desired checkerboard pattern. When the device is initialized the controller regulates the input voltage

which comes from either the on-board USB connection or through a 5V battery source while the grid temperature is monitored with a thermocouple and the ambient temperature is measured via an infrared room temperature sensor. Since the grid is maintained at a fixed differential from the ambient temperature the grid is stable and always visible in the thermal imager.

The wire selected was 39 AWG Magnetic wire because the small diameter (d=0.0897 mm) will reduce image distortion as well as not interfering with the edge detection in the RGB camera calibration images. The length of the wire used, L= 2.44 m, resulted in an overall resistance through the wire of 6.7 Ω in a 7x9 square checkerboard grid with a grid spacing of 15mm. With consideration to the safety of the device a maximum allowable current was set to be less than 1 A thus, a 5V DC battery was selected for the device. To minimize the temperature measurement delay in the system a Type-K Thermocouple was selected to measure the temperature of the wire grid while the DS18B20 one wire temperature sensor was used to measure the ambient temperature. Figure 2.4 shows the wiring diagram used as well as the implementation of these components in the final design.

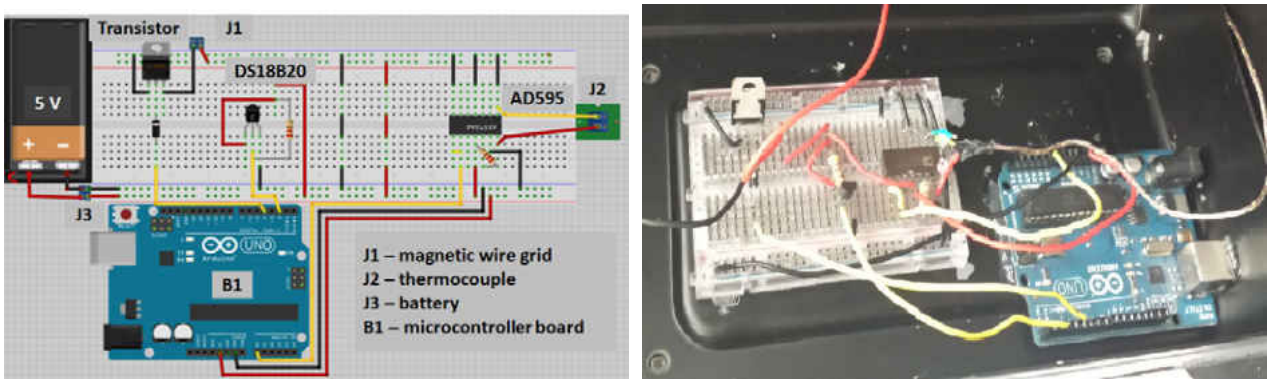

(a) Design of Control grid Circuit

(b) Hardware implementation

Figure 2.4: Thermal Calibration Grid Implementation

2.2.3 Stereo Camera Calibration

The Caltech toolbox includes a stereo camera calibration toolbox is also included and it provides a means of calculating the rotation and translation matrices between two the origins of cameras for the right RGB camera to the left RGB camera and the left RGB camera to the thermal camera, $R_{RC \to LC}$ and $R_{LC \to Thermal}$ respectively, relates the coordinate origins of the cameras using only the individual calibration results of the webcams and thermal imager. The benefit of this method is that the matrices can be calculated without needing to measure the locations of the camera focal points, which can be difficult as the focal point is not a physical point in space. The stereo calibration toolbox uses the checkerboard intersection point locations in the calibration results from both cameras to locate the position and rotation of the right camera with respect to the left camera. The toolbox output is the rotation matrix and translation vector for the right camera location with respect to the left

camera location. These can be combined to form a homogeneous transformation matrix as follows,

$$M = \begin{pmatrix} \Omega_{3\times3} & T_{3\times1} \\ 0_{1\times3} & 1 \end{pmatrix}$$

where Ω is the rotation matrix and T is the translation vector in the x, y, and z directions. This matrix is used to triangulate the 3-D position of a point of interest in the left camera frame coordinates. It also provides an easy means of correlating 3-D points in space between coordinate systems via simple matrix multiplication.

2.3 Stereo Camera Correlation

The simplest form of the correlation problem is that of a point in a single stereo pair being correlated to the thermal imager coordinate frame. This representation can be seen below where *Point 1* is found through point triangulation to have [*x,y,z*] coordinates in the *LC1* Frame. This triangulation process is shown by the arrow between the *LC1* and *RC1* coordinate frames using the transformation matrix $R_{RC1\rightarrow LC1}$ which was found during the stereo camera calibration process. The dashed lines from the RGB cameras are the projected image points found though triangulation between and the line from the thermal camera projected point in the thermal camera reference frame.

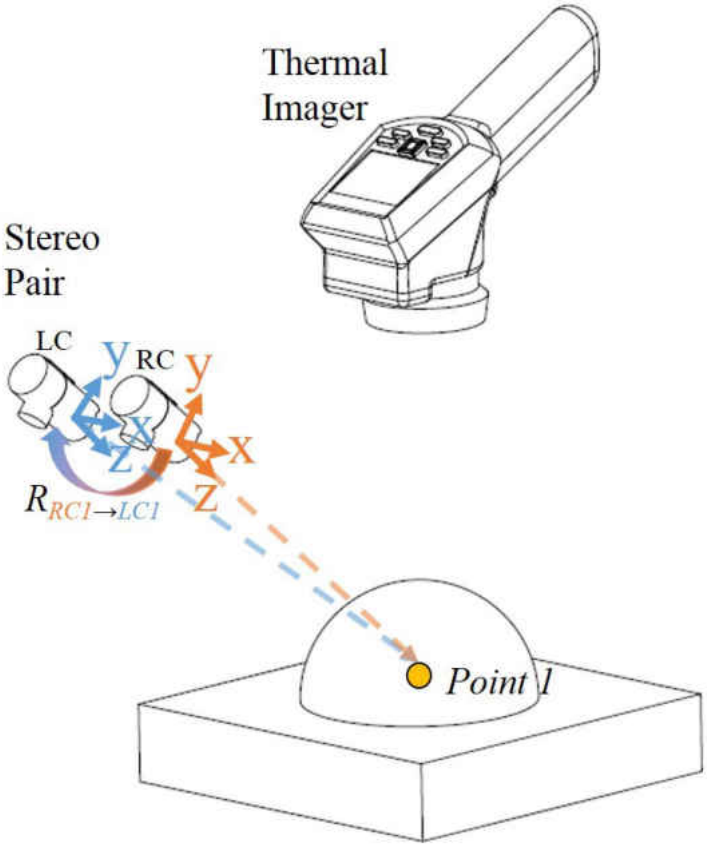

Figure 2.5: Single Stereo Pair triangulation with camera origins and point projections.

With the point coordinates in the left camera frame it is now possible to locate the coordinates of the point in the thermal imager coordinate using the $R_{LC1 \rightarrow thermal}$ coordinate transformation found from stereo calibration.

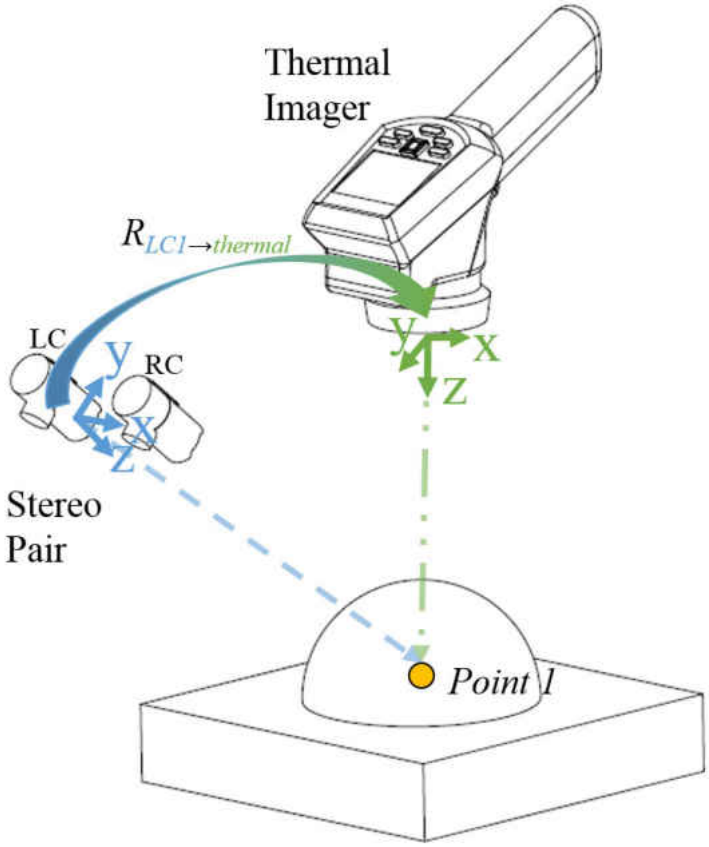

Figure 2.6: Single Stereo Pair to thermal camera correlation with camera origins and point projections.

The representation of this process is simply a series of matrix multiplication operations which is easy to implement for multiple points of interest while remaining computationally efficient. This can be easily seen in the following equations.

$$N = \begin{bmatrix} x_1 & x_2 & \dots & x_n \\ y_1 & y_2 & \dots & y_n \\ z_1 & z_2 & \dots & z_n \\ 1 & 1 & \dots & 1 \end{bmatrix}_{LC(i)} \tag{2.3.1}$$

where N is the coordinates of n points of interest found through triangulation in the LC camera frame. From this the following matrix multiplication can be conducted resulting in the points of interest in the thermal camera coordinate frame.

$$[P_{thermal}]_{4\times n} = [R_{LC\rightarrow thermal}]_{3\times 4} \times [N_{LC}]_{4\times n} + [T_{LC\rightarrow thermal}]_{3\times 1} \tag{2.3.2}$$

Resulting in:

$$P = \begin{bmatrix} x_1 & x_2 & \dots & x_n \\ y_1 & y_2 & \dots & y_n \\ z_1 & z_2 & \dots & z_n \\ 1 & 1 & \dots & 1 \end{bmatrix}_{thermal} \tag{2.3.3}$$

With these points in the thermal imager coordinate frame we can use the camera focal lengths in the x and y direction to locate the i^{th} pixel locations of n points of interest in the following equation.

$$\begin{bmatrix} x_i \\ y_i \end{bmatrix}_{pixel} = \begin{bmatrix} \frac{P_x(i) f_{cx}}{P_z(i)} \\ \frac{P_y(i) f_{cy}}{P_z(i)} \end{bmatrix} \tag{2.3.4}$$

The benefit of this method is that it can easily be expanded to being used with i camera pairs to locate n points on a surface, which can be seen below in figure 2.7.

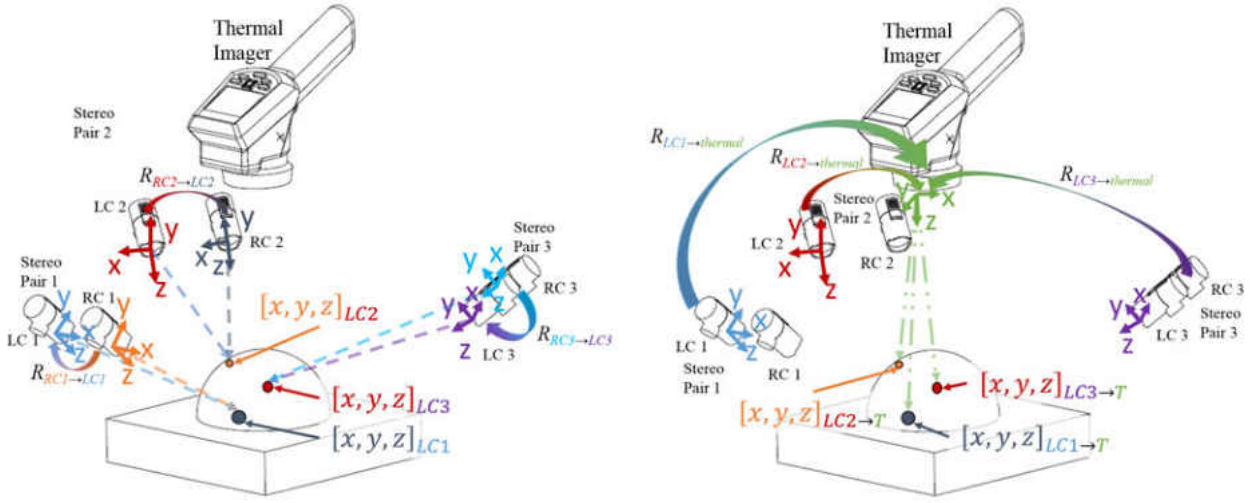

(a) Stereo Camera Triangulation

(b) Thermal Camera Correlation

Figure 2.7: Two-Step Camera Correlation for Temperature Measurement

To accomplish this, the only necessary change is to alter equation 2.3.2 to use the proper transformation matrices for the camera pair which has the best field of view of the point of interest. This change can be seen below.

$$[P_{thermal}]_{4\times n} = [R_{LC(l)\to thermal}]_{3\times 4} \times [N_{LC(l)}]_{4\times n} + [T_{LC(l)\to thermal}]_{3\times 1} \tag{2.3.5}$$

where l=1,2,...,i

with these points being represented in the thermal imager coordinate frame equation 2.3.4 is still valid and does not require any changes to locate the pixel locations of the points of interest in the thermal image. With these pixel locations a simple linear interpolation technique can be used to calculate the temperature information of the points based on the intensity of the grayscale pixel value.

$$T(i) = (T_{ub} - T_{lb}) \times \frac{U(i)}{255} + T_{lb} \tag{2.3.6}$$

where *U(i)* is the pixel intensity value for the i^{th} point of interest, T_{lb} is the lower bound temperature set on the thermal imager and T_{ub} is the upper bound temperature set on the thermal imager. This method of temperature calculation is computationally efficient and does not require an expensive software package to monitor real time temperature information interfaced with Matlab.

CHAPTER 3

ELECTRICAL SYSTEM FOR MONITORING SHAPE MEMORY POLYMER STRUCTURES

Though an electrical system was previously designed for use in the shape memory polymer testbed, it was not well suited for use with structures capable of actuation in the 3-D space. The nature of the structures we wish to analyze require much flexibility in the testbed so the electrical system must also be flexible. With this in mind, several key improvements were made including: increasing sensor accuracy, sense voltage and current in real time, maintain temperature measurement accuracy, increase electrical system stability, and allow for expansion of electrical components.

3.1 Electrical Specifications

The electrical subsystem that was initially used was optimized for analyzing a bar sample actuating in a single plane. To adjust the system for more complex structures increasing the sensor accuracy requirements of the system would be essential for control applications since the dynamics of the material are more complex and simple PID control would no longer be

able to control the material deflection. The current sensor accuracy was changed to being less than .01 A and voltage measurements will be attained by adding a potential divider to calculate the voltage being experienced by the sample. The voltage in the sample is calculated using the following.

$$V_{sample} = \frac{R_2}{R_1 + R_2} \times V_{pin} \tag{3.1.1}$$

with R_1 and R_2 being the resistors which make up the potential divider, and V_{pin} is the voltage read by the Arduino analog pin. The analog to digital converter on the Arduino is limited to values between 0-1023 which affects the accuracy of the measurements which can be taken by the potential divider.

$$Accuracy = \frac{V_{max}}{1024} \tag{3.1.2}$$

where

$$V_{max} = \frac{5.0 \times (R_1 + R_2)}{R_2} \tag{3.1.3}$$

with equation 3.1.3 and the maximum supply voltage of 35 Volts selected to prevent damage to the Arduino through over-voltage, it is possible to calculate the values of R_1 and R_2 to increase the accuracy of the voltage measurement. To reduce any possible errors from the potential divider measurement a large impedance is needed. For ease of calculation R_2 is assumed to be 1 MΩ so using equation 3.1.3 with the substituted values we find that.

$$35V = \frac{5.0V \times (R_1 + 1000000\Omega)}{1000000\Omega} \tag{3.1.4}$$

$$R_1 = 6000000\Omega \tag{3.1.5}$$

The accuracy of the potential divider can similarly be found from equation 3.1.2 to be,

$$Accuracy = \frac{35V}{1024} = 0.0342V/Step \tag{3.1.6}$$

Which will be sufficient as our voltage control is to 0.1 V and the voltage is simply for external monitoring and not actually used in the deflection control. To accommodate for standard resistor values the values for R_1 and R_2 are chosen to be 6.2 MΩ and 1 MΩ which will adjust the maximum voltage value to 36 V and the accuracy to 0.0352 *V/Step*. To display the values of current and voltage in real time an expansion board which has two 4 digit common cathode 7 segment displays was implemented with an MAX7221 LED display driver. The display driver is necessary because in order to operate all digits of the display it would require the use of 64 digital pins on the arduino to run individual displays, however, when the display driver is used, the number of digital pins required is reduced to 4. The schematic for this expansion can be seen below.

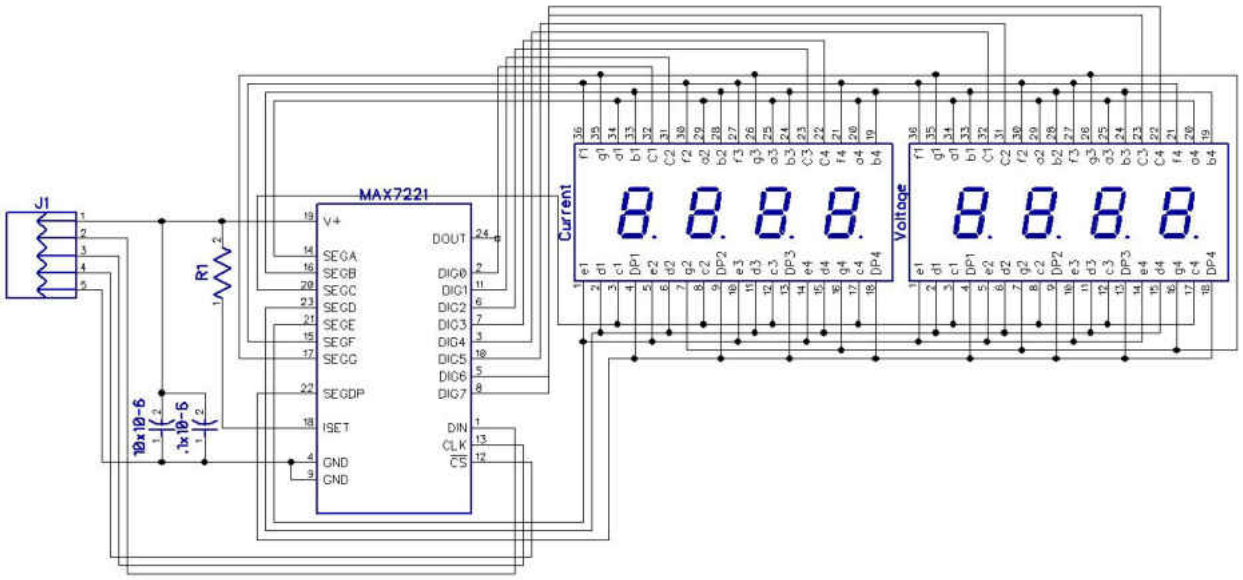

Figure 3.1: 7 Segment Display Schematic

Where *J1* consists of a 5 pin connector which leads to 1) 5 V Arduino Power, 2-4) are Arduino digital pins and 5) is the 5 V ground on the Arduino. For more complex structures it may become important to be able to actuate multiple surfaces of the structure simultaneously for greater control of the overall deflection shape. To accommodate that the electrical system has been designed to use another expansion board with 4 Type-P MosFETs on it which is wired to a 74HC4051N 8-Channel De-Multiplexer. This configuration allows for up to 8 independent heating channels, though more could be easily added in the future. All of these channels share a path to ground so only one Pulse-width Modulation transistor and command is required which greatly reduces the complexity of the circuits significantly. The schematic for the channel selection circuit can be seen below.

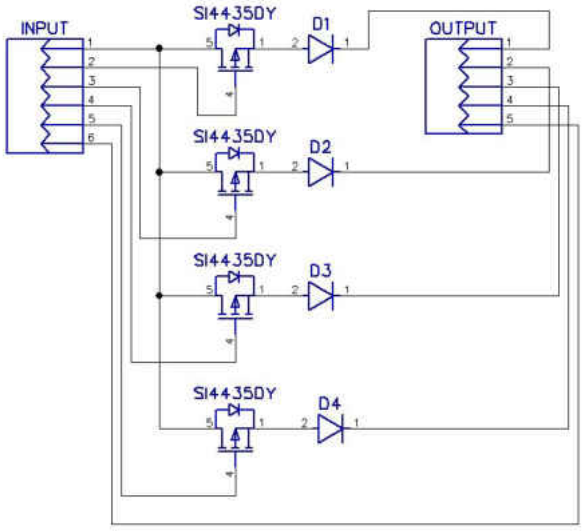

Figure 3.2: Power Channel Selection Schematic

Where *Input* consists of a 6 pin connector which leads to 1) Pwm Ground , 2-5) are de-multiplexer pins and 6) is the 30 V positive terminal from the power supply. The *Output* consists of a 5 pin connector which leads to 1-4) ground terminal for shape memory polymer structure structure heating zones and 5) is the positive terminal for all shape memory polymer structure heating zones. The combination of all of these subsystems into a single cohesive circuit was needed to be implemented into the testbed to improve performance of the testbed. The complete system could be used to develop an Arduino shield with breakout boards for the power channel selection and 7 segment display board, the combination of these schematics can be seen below in the figure.

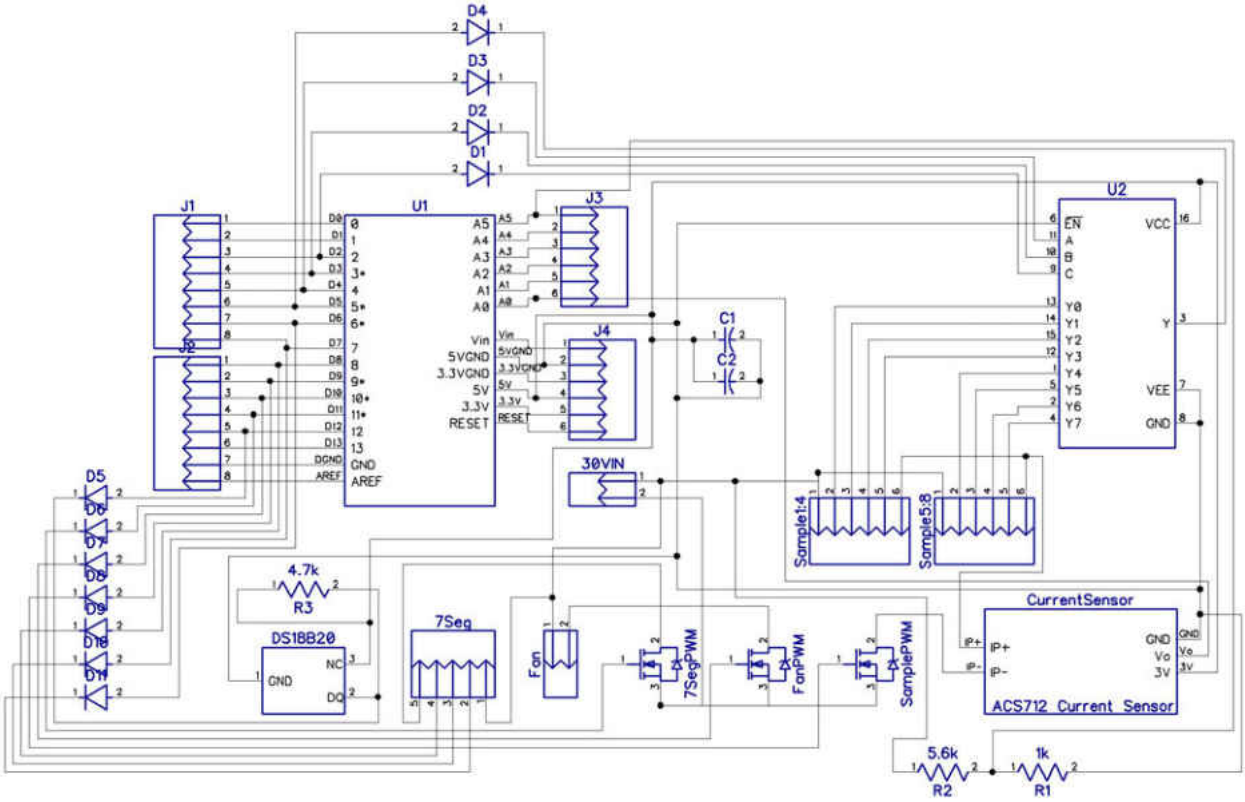

Figure 3.3: Electrical Subsystem Schematic

where *J1-J4* are the pins to the Arduino in an Arduino shield configuration, *Sample 1:4* and *Sample 5:8* are the interfaces to the power selection breakout boards and *7Seg* is the interface of the 7 segment display breakout board. The final implementation uses diodes to prevent damage to the arduino and combines all of subsystems into a single cohesive circuit.

3.2 PCB Design for Electrical System

One of the main objectives of the electrical subsystem redesign was that the stability of the circuits needed to be drastically improved. Before the redesign all of the circuits were bread boarded on a large breadboard that was very sensitive to bumping which would cause the calibration of the current sensor to become invalid. The previous iteration of the circuits can be seen below in figure 3.4.

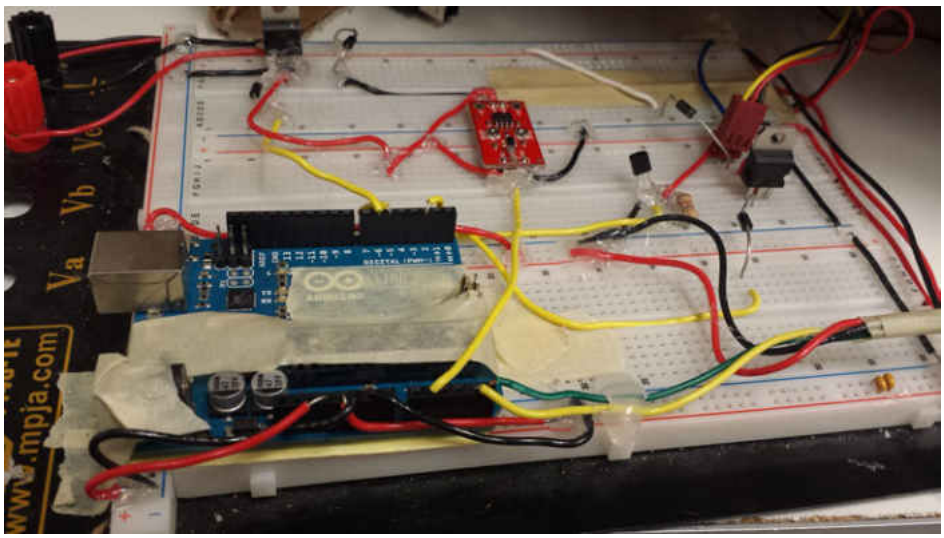

Figure 3.4: Previous Testbed Circuit

The subsystems which were discussed earlier needed to be implemented in a stable platform which would allow for the testbed to be used for many so a printed circuit board (PCB) was designed to serve as an Arduino shield for the testbed. In addition to the shield PCB, other PCBs would need to be made to house the heating channel and 7 segment display breakout boards. The boards were designed to have the smallest form factors possible to

enable the components to fit into a small project box to contain them to prevent damage to the electrical components of the testbed. The preliminary designs of the PCBs can be seen below in figure 3.5.

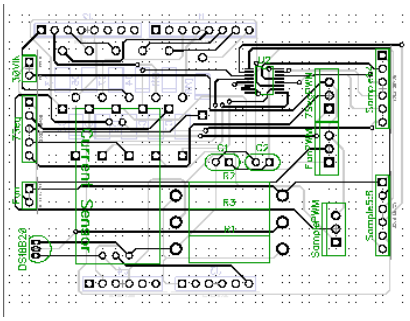

(a) Arduino Shield PCB Schematic

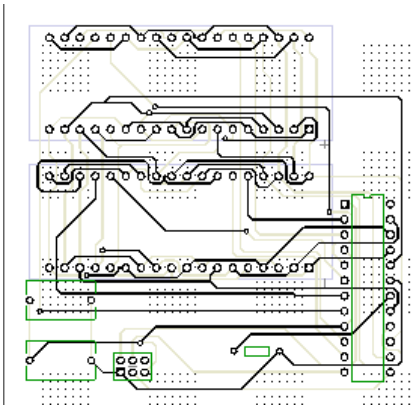

(b) 7 Segment Display PCB Schematic

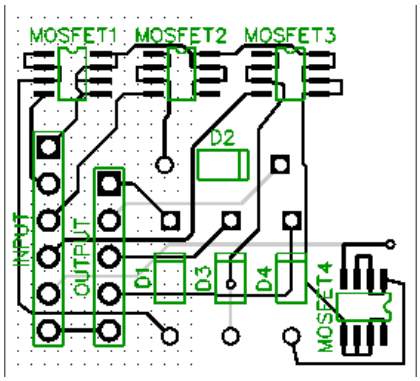

(c) Heating Channel PCB Schematic

Figure 3.5: PCB Schematics for SMP Testbed

The software used to create these schematics, DipTrace, can also be used to create renderings of the PCBs to fit them into solid models for analysis. The rendering of the PCBs above can be seen below in figure 3.6. Though these designs were completed the production of the PCBs was not possible through a professional service so the different PCBs were bread boarded on separate breadboards to simulate the desired functionalities of the electric subsystem and verify the schematics perform as designed. This verification could be used as validation to professionally manufacture the PCBs in the future. The breadboard simulated circuits can be seen in figure 3.7.

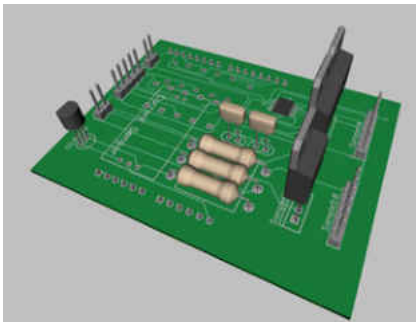

(a) Arduino Shield PCB Rendering

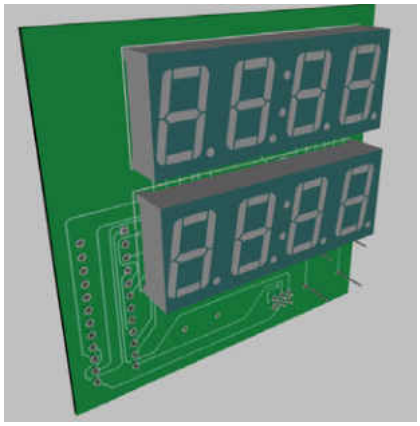

(b) 7 Segment Display PCB Rendering

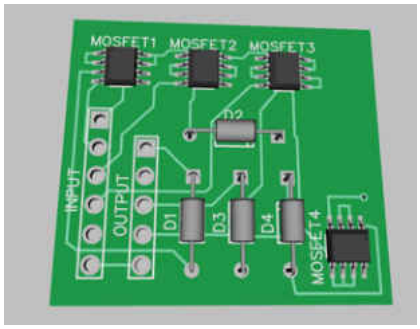

(c) Heating Channel PCB Rendering

Figure 3.6: PCB Schematics for SMP Testbed

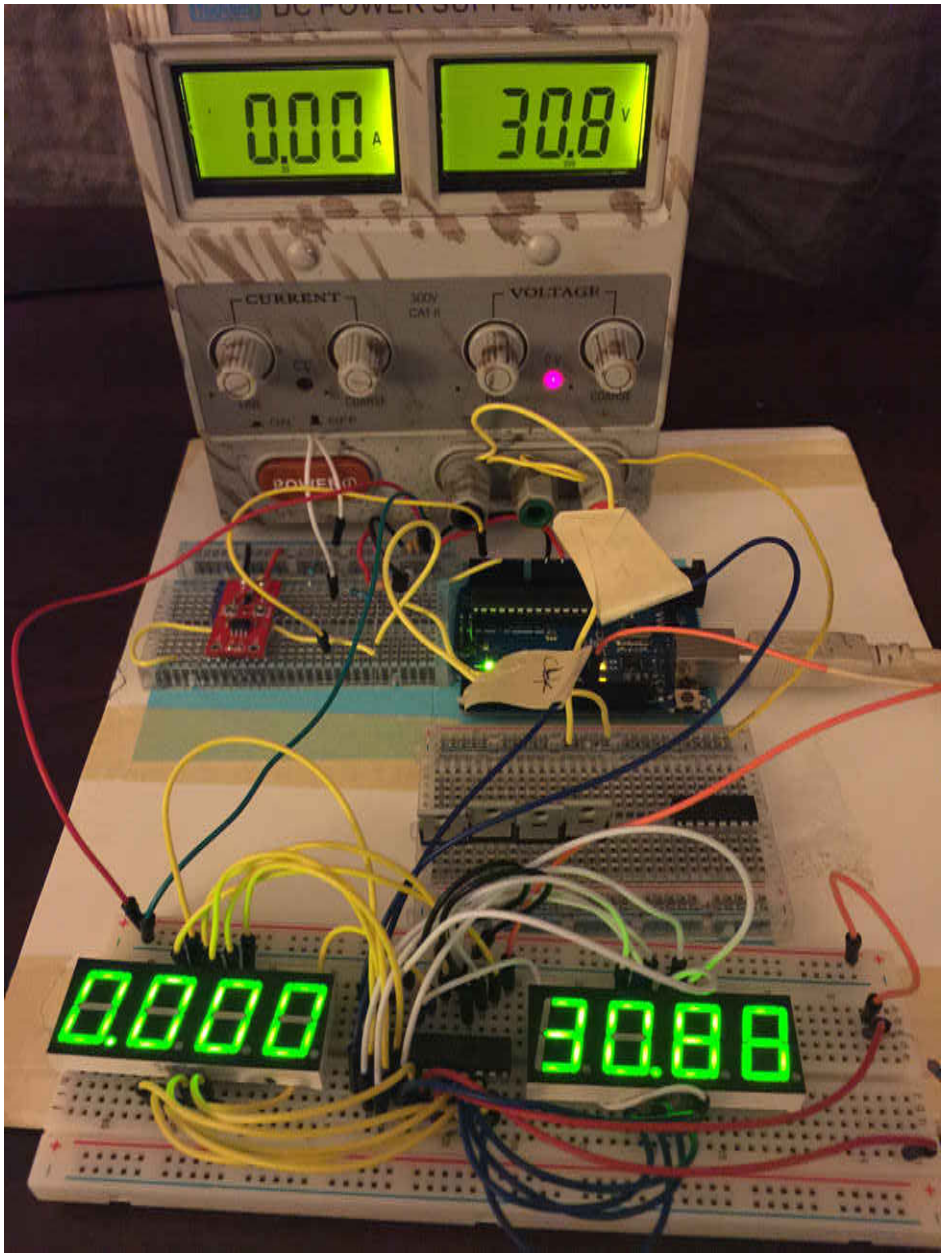

Figure 3.7: Breadboard of Final PCB Design

CHAPTER 4

SOFTWARE FOR MONITORING SHAPE MEMORY POLYMER STRUCTURES

The Graphical User Interface (GUI) which was previously implemented in the testbed was designed with only tracking the points from a single pair of cameras which can be seen below.

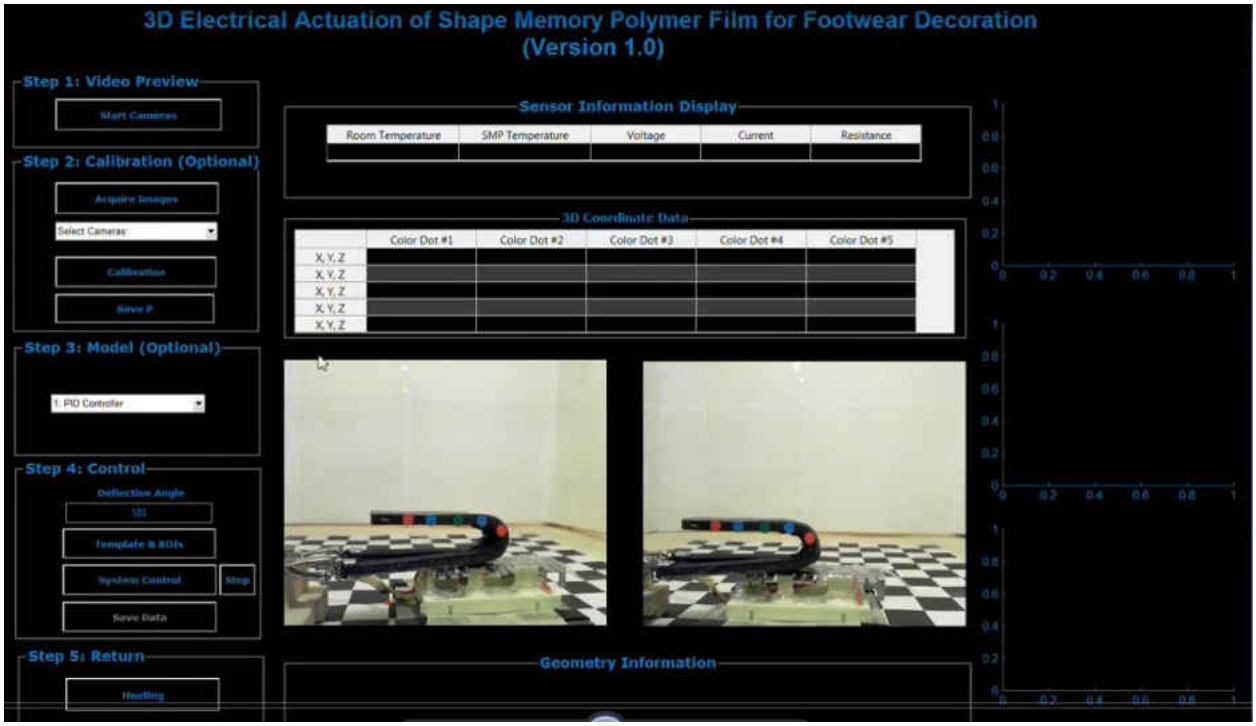

Figure 4.1: Former GUI Design

The GUI needed to be completely redesigned with the implementation of the 3 stereo pair and thermal camera to accommodate the increased functionality of the system. When this redesign was conducted several performance specifications and goals for the new GUI were established.

4.1 GUI Specifications and Goals

The previous GUI had some aspects which were still desirable in the new GUI design. Some of these were the simple button interface, simultaneous camera previews, Temperature Display, and Electrical information display. In addition to these existing features, several more would be added such as integrated calibration toolbox commands, 7 camera preview windows, stop camera buttons, thermal modeling GUI pop-out, maximum temperature display and sample rate display.

The main concern with adding all of these functionalities to the GUI was that it would result in a decrease in performance. The previous GUI was capable of tracking points in two cameras at a rate of 4.5 Hz which was below the desirable rate of 5 Hz but still sufficient for our experimental process. To compensate for the inevitable slowing of the process by adding more cameras, a smarter method of serial communications was devised which would only read or write when necessary instead of reading and writing whenever the serial communication occurs. Since 95% of the calculation operations for the GUI were taken up by serial communications this greatly increased the speed of the GUI to over 10 Hz with

proper variable allocation schemes used. To increase the stability and prevent fluctuations in measurement speed the sampling rate is fixed at 8 Hz which exceeds the desired 5 Hz. For the Thermal Modeling GUI no tracking occurs so it is possible to have the GUI operate at 15 Hz which provides higher resolution for the solver which is desired.

The main goals for the GUI are as follows, provide a method for easy stereo camera calibration, be able to find the temperature of points of interest in real time, track geometry information in real time, track up to 5 points of interest in each camera pair image plane and to be easy to be understand and use by the operator.

4.2 GUI Implementation

To create the GUI, the integrated GUI creator and editor in Matlab GUIDE was used. This tool provides an easy to use way to layout and generate Matlab code for a GUI, then simply insert the code that should be executed on button presses or changed by text input boxes. The generated overall GUI can be seen in the figure below with the control panel on the left side and the video preview area on the right. This layout sticks to the original layout of the GUI while increasing the functionality of the testbed and allowing for more flexibility while conducting experiments.

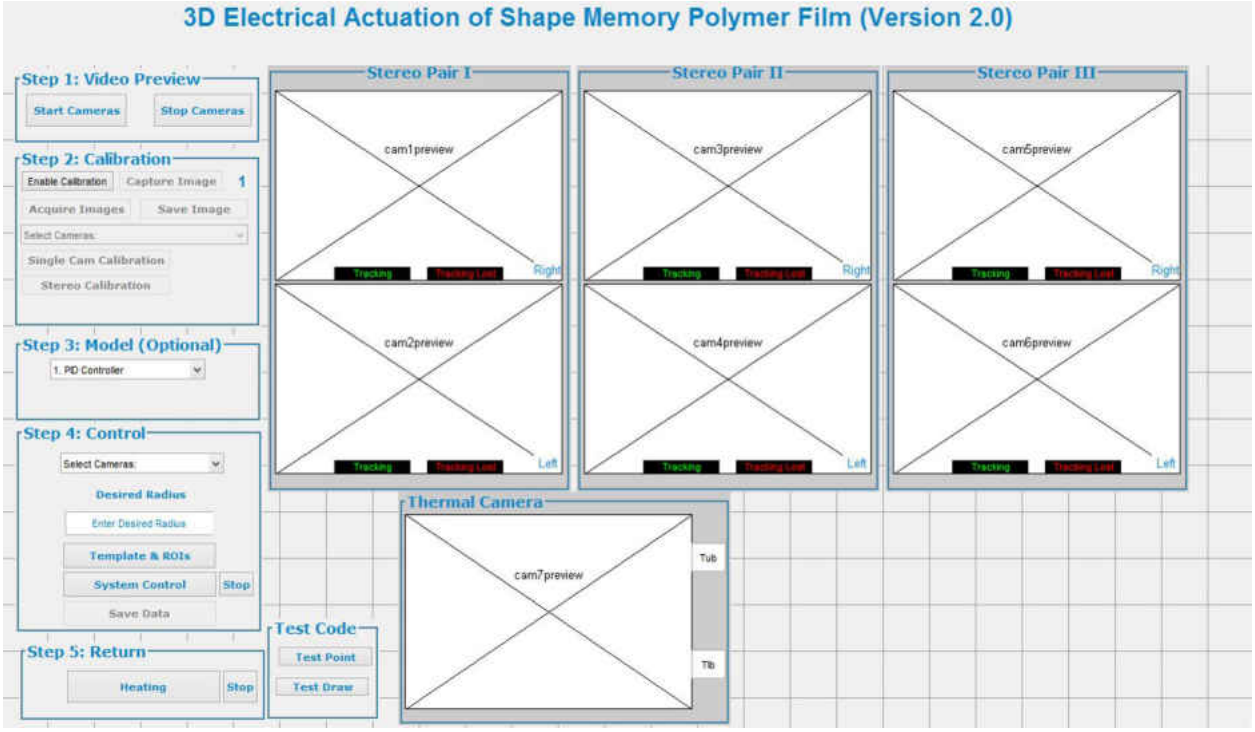

Figure 4.2: Overall GUI Layout

The first block of the GUI is the *Step 1: Video Preview Block* shown below, it contains two pushbuttons which allow the user to both start and stop the cameras in the preview windows. The ability to start and stop the cameras is important because during tracking circles are plotted on the image preview and stopping the cameras allows these circles to be reset for additional experiment runs.

Figure 4.3: Video Control GUI Block

The second block of the GUI is the *Step 2: Calibration* block shown below, it contains a toggle button to activate calibration and several buttons and drop-downs which are only accessible after the *Enable Calibration* button is pressed. After this button is pressed the window allows the user to capture 20 images of a checkerboard grid using the preview windows to ensure the checkerboard is within the image plane in all cameras. With the calibration images, it is possible to select cameras to run the single camera calibration from the Caltech Toolbox [30]. After all of the calibration variables have been found, the stereo calibration between the stereo pairs and thermal imager can be conducted using a different calibration tool within the Caltech Toolbox. Using an integrated Calibration tool greatly reduces the amount of time to calibrate the cameras for experiments.

Figure 4.4: Calibration GUI Block

The next two blocks of the GUI are the *Step 3: Model* and *Step 4: Control* are shown below. These blocks provide a method to launch the thermal modeling GUI or select a model for the controller to be used, currently only a PID controller is available for use. The *Select*

Cameras dropdown in the *Step 4: Control* block allows for the user to select which pair of stereo cameras will be used as well as any combination of the three together. The *Desired Radius* editable text box allows the user to define the desired radius for the controller to control towards. The *Template & ROIs* button allows the user to establish the templates and regions of interest for the tracking algorithm. With the templates saved the user can now start the actuation process by clicking the *System Control* button and are able to stop it at any time with the *Stop* button. Once the actuation is complete either via reaching the desired radius or being stopped the *Save Data* button will become active and allow for the experiment data to be saved.

Figure 4.5: Model and Control GUI Block

The final block for user interaction is the *Step 5: Return* block which is shown below. This block allows the user to reheat the SMP structure to reset it to a temporary configuration for the next experiment. This step utilizes the maximum surface temperature to ensure that no damage is caused to the material and activates the fans afterwards to cool the sample back down to room temperature prior to the next experiment start. This block also features a *Stop* button to stop the heating at any time and starting the fans to prevent damage to the SMP structures.

Figure 4.6: Reheat GUI Block

The other section of the GUI is the video preview window which can be seen below. This area of the GUI provides the video previews for all 6 webcams organized by stereo pairs and the thermal imager in the bottom. Each camera in the stereo pair has a tracking status indicator at the bottom of it which allows the user to know the tracking status if the circles are not being plotted on the preview windows. The thermal imager also features two editable text boxes which allow the user to set the upper and lower limits of the thermal imager scale for the software interpolation to determine the temperature of the points of interest in the imager.

Figure 4.7: Video Preview GUI Blocks

CHAPTER 5

IMPROVEMENTS AND APPLICATIONS FOR SHAPE MEMORY POLYMER TESTBED

5.1 Summary of Testbed Improvements

5.1.1 Comparison to Sivilli Testbed

The testbed developed is the third iteration in a series of testbeds with the first of which was programmed with only two webcams and was programmed in labView [13]. This testbed was the foundation for many of the integrated features of the 3D vision testbed developed in this paper including the tracking algorithm development and the preliminary hardware and circuit designs. A comparison of the initial hardware setup and the current testbed configuration can be seen below.

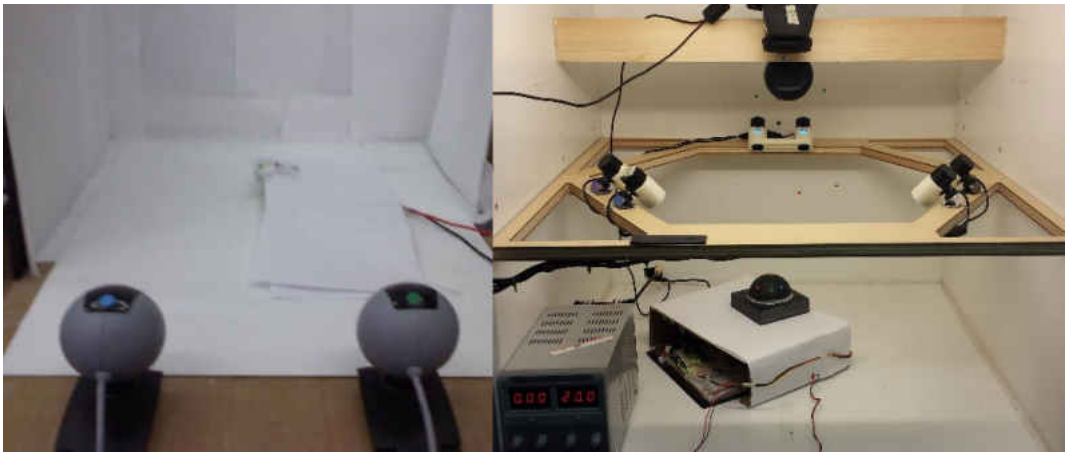

Figure 5.1: Comparison of Sivilli Testbed to Current Testbed[29]

It can be seen that the previous version of the testbed did not have rigid mounts for the cameras and also did not include the thermal imager. The new testbed does have rigid mounting of all cameras. The cameras in the Sivilli testbed also only had a maximum resolution of 640 x 480 which significantly reduces the tracking capabilities as it lowers the pixel density of the tracking template. In the current version of the testbed the camera resolution was increased to 1280 x 720 which results in a pixel density four times larger than that of the previous webcam configuration. The increase in camera resolution should decrease the tracking frequency due to increased CPU time required for image processing, but the new testbed actually has significantly higher sampling frequencies than the Sivilli testbed. This performance increase can be attributed to several key improvements in the software design. First the GUI for the new testbed was programmed using LabView, whereas the GUI for the new testbed was programmed in Matlab which has better image processing algorithms. It should be noted that the GUI developed in the LabView environment was not capable of

conducting stereoscopic geometry reconstruction which greatly reduces the flexibility of this version of the testbed. Secondly, the serial communication between the Arduino and Matlab was optimized to significantly reduce the CPU time required for this necessary communication. This change allows the new testbed to operate at sampling frequencies higher than 10 Hz.

5.1.2 Comparison to the Shen Testbed

After the Sivilli testbed was developed the testbed was upgraded to integrate stereoscopic reconstruction as well as move the GUI to Matlab. There were also several upgrades to the electronic and hardware systems. Improved cameras were added to the testbed which would increase their tracking accuracy though the GUI developed was only capable of running the tracking code at 3 Hz. The thermal camera had still not been integrated into the testbed. A comparison between the Shen testbed and the testbed developed in this paper can be seen below.

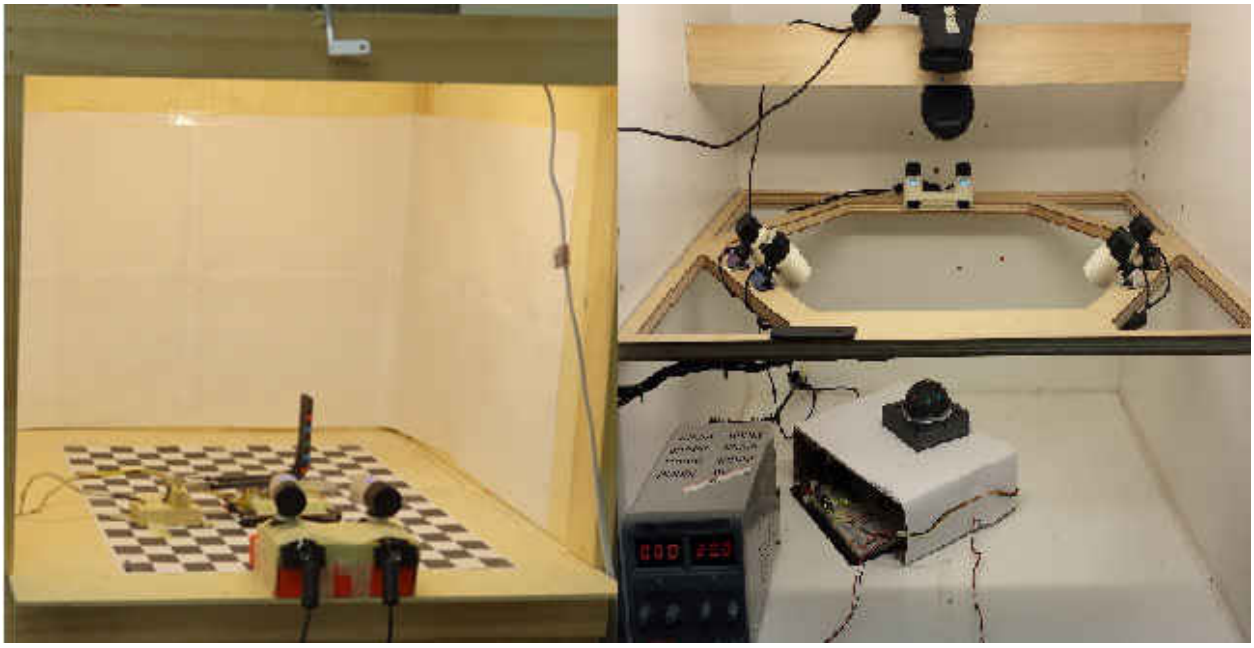

Figure 5.2: Comparison of Shen Testbed to Current Testbed[29]

The testbed was in this condition when I began working on developing the 3D vision system. It is clear to see that this testbed was the inspiration for the current version, though it did have some significant issues with it. The main issue with the Shen testbed was that it was only capable of measuring 2D motion of the SMP samples. The addition of four more webcams would allow the new version of the testbed to be capable of measuring the 3D motion of SMP samples. The Shen version of the testbed was also very vulnerable to calibration errors as the cameras could be moved if the cords were moved or the box containing them was bumped. This problem was fixed through the development of the printed camera holders which are integrated into the 3D vision testbed.

5.2 Applications of Shape Memory Polymer Testbed

This testbed was developed with the primary application being shape memory polymer structure research. The research focus involves thermal modeling of shape memory polymer composites for more accurate control of the structures actuation. Another application that was focused on was the tracking and correlation of shape memory polymer structures, which has the direct application of being able to control the actuation based on the vision and temperature information captured in the testbed in real time. It should be noted that the testbed has other applications in shape memory polymer actuation as well as other smart materials such as shape memory alloys and piezoelectrics. The direct image correlation also has applications in any system where accurate non-contact temperature measurements are required. The GUI for this version of the testbed did not have an integrated calibration function and required images to be acquired externally to the GUI which decreased efficiency while conducting calibration. These deficiencies in the Shen testbed were some things that became constraints when designing the new 3D vision testbed.

5.2.1 Thermal Modeling of Shape Memory Polymer Composites

One main issue that occurs during shape memory polymer structure research is that once a composite structure is created the thermal properties of the structure. Being able to identify or estimate values for the new thermal properties of the composites will allow for a greater

understanding of how the material behaves and opens up the actuation for better control using a model based controller. The process of identifying the thermal constants uses a finite element formulation to estimate the heat transfer occurring in volume elements within the composite structure. To accomplish this an element on the surface is chosen to be 1 pixel in the thermal imager image and the heat transfer to surrounding elements is estimated by selecting the 4 pixels around it as shown below.

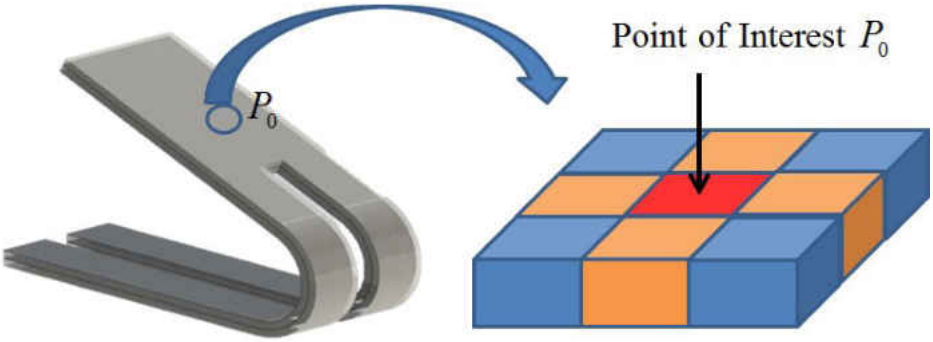

Figure 5.3: Finite Element Configuration for Thermal Constant Identification[29]

The red center is the pixel which is chosen to be the point of interest and the four orange sections adjacent to the point of interest are the elements which conduction heat transfer occurs in our finite element model. The overall heat transfer for the point of interest, which can be seen below, consists of convection and radiation heat transfer from the upper and lower surfaces of structure, conduction heat transfer to the adjacent elements and heat generation within the carbon nanopaper layer of the composite.

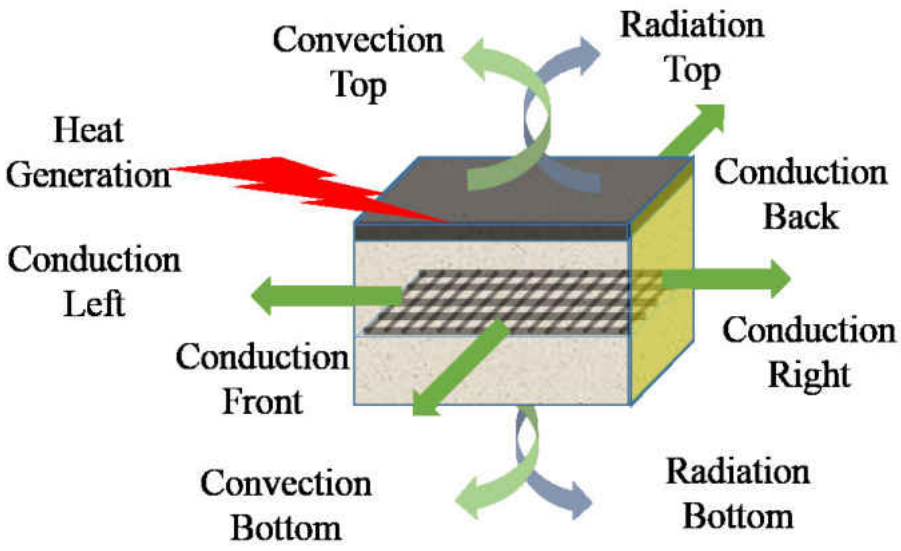

Figure 5.4: Element of Interest Heat Transfer Summary[29]

To collect the data required for identification an experimental process was designed which would allow the user to select a point of interest on the surface and heat the structure at different voltages to increase the accuracy of the identified constants. To accomplish this, an easy to use GUI was developed which would automatically run the experiments on a set range of voltages and number of experience. This GUI is launched out of the main GUI from the model select dropdown menu in the *Step 3* block. The GUI can be seen below in Figure 5.5.

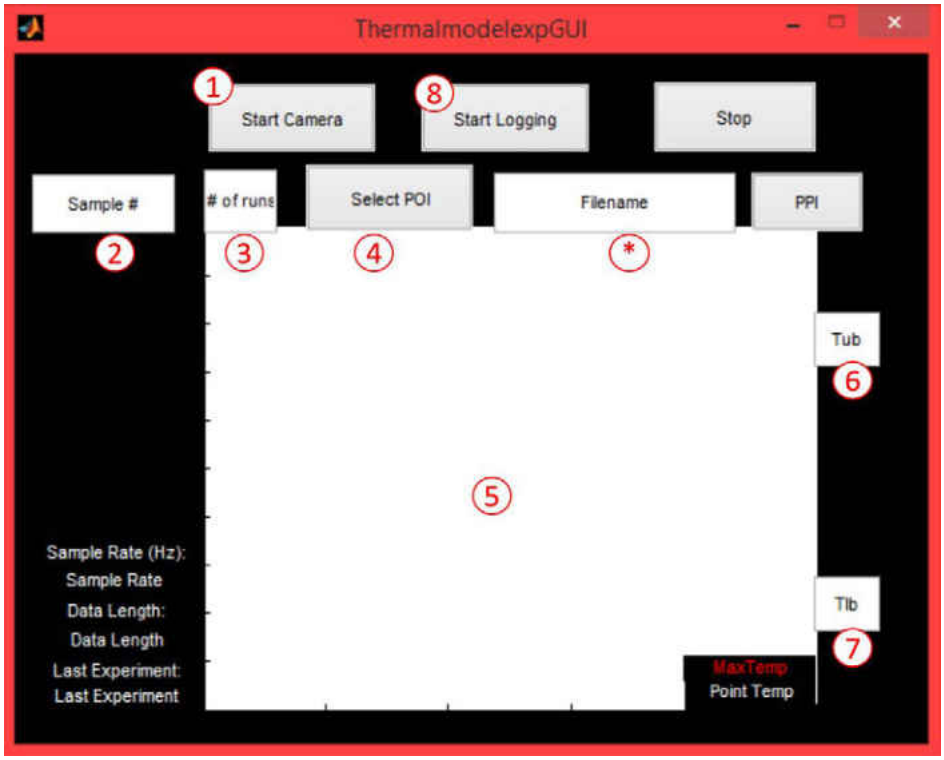

Figure 5.5: GUI for Thermal Constant Identification

In the GUI, *1* starts the thermal imager in the GUI window while closing the preview active in the main GUI, *2* changes the sample # in the data structure of the experiment, *3* changes the number of runs at each voltage step for the experiment with they default being 5 runs, *4* manually selects the point of interest on the sample,*5* is the thermal imager preview window, *6 & 7* are the upper and lower bounds of the thermal imager temperature scale and the *Stop* button stops the experiment and saves the data. The GUI also keeps track of the data length, sample rate, and maximum temperature to prevent damage to the samples during experiments and to determine if the data collected will be usable. As these experiments can consist of 35 or more runs taking up to 4 hours the process of heating and cooling was

automated using the integrated fans to increase the speed of cooling and also ensure uniform starting temperatures for the experiments. The fan control is governed by the temperature of the point of interest and cools the structure until the temperature is below 23°. At the conclusion of the experiment set the GUI compiles the data into a single .zip file and emails it to the user notifying them of completion. This "start and forget" methodology frees up the user to do other things during an experiment which does not necessarily require constant supervision. The data obtained, in the form of an $n \times 9$ matrix with n being the data length consisting of time, current, control command, ambient temperature, POI temperature, top temperature, right temperature, bottom temperature and left temperature. This data is used in a nonlinear solver to determine the coefficients of specific heat and thermal conductivity as seen in [31].

5.2.2 Tracking and Correlation of Shape Memory Polymer Structures

The tracking and correlation of points of interest is one of the most important applications of the platform, with its accuracy affecting the accuracy of all experiments that take place within the testbed. The first configuration used to test the tracking and correlation is a stationary structure test. This allowed us to verify that the tracking is able to find the initial point of interest and stabilize around that point and that the point correlation between the RGB webcams and the thermal imager is within the requirements for the platform. Through this experiment, the location of the point in the RGB camera frame is within the 1mm

measurement tolerance established and the pixel travel is within the 5-pixel tolerance for the platform. These points were then correlated to the thermal imager and plotted on the image to verify the location. A cold rod is used to point on the surface and mark these points manually to compare to the correlated results. The resulting error from this process is around 1 pixel, which is lower than the 2-pixel tolerance set for the platform. This showed that if the tracking results are correct in the RGB cameras, the correlation to the thermal imager will be correct as well.

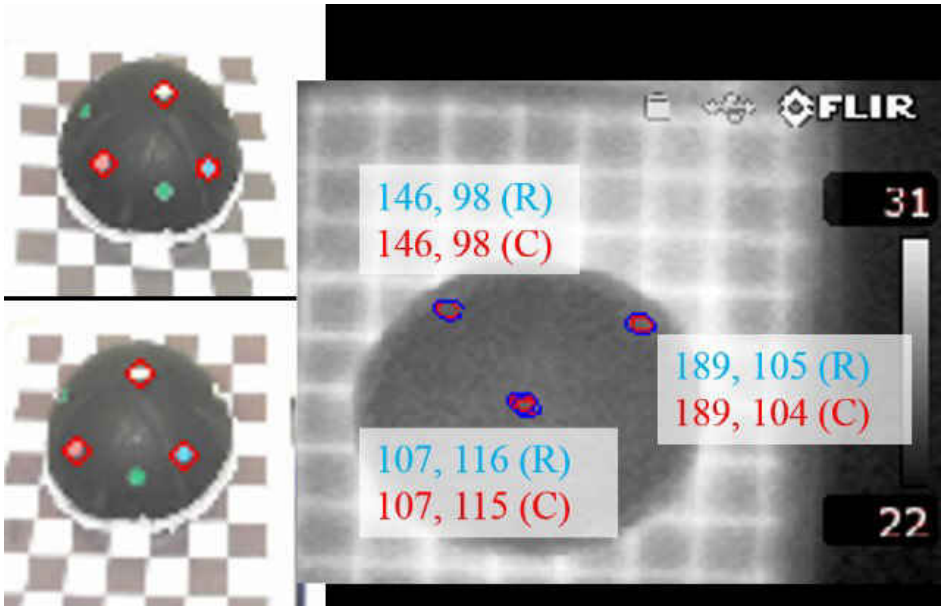

Figure 5.6: Stationary structure tracking with correlation[29]

The next step is to conduct a similar experiment with a moving SNS to verify that the platform is capable of monitoring moving structures. Once again 3 points were tracked by a stereo pair of webcams but this time on a moving SMP bar structure activated at 15 V DC. A second stereo pair is used to simultaneously provide a reference for the correlation pixel

locations. The tracking of the sample is still within the desired specifications for both location and speed with an average sampling rate of 5.1 Hz, which exceeds the 4 Hz requirement with the GUI running and the correlation results were within the 2-pixel tolerance of the reference points which were checked with the cold rod at the beginning and the end of the motion to verify the accuracy of the reference plot.

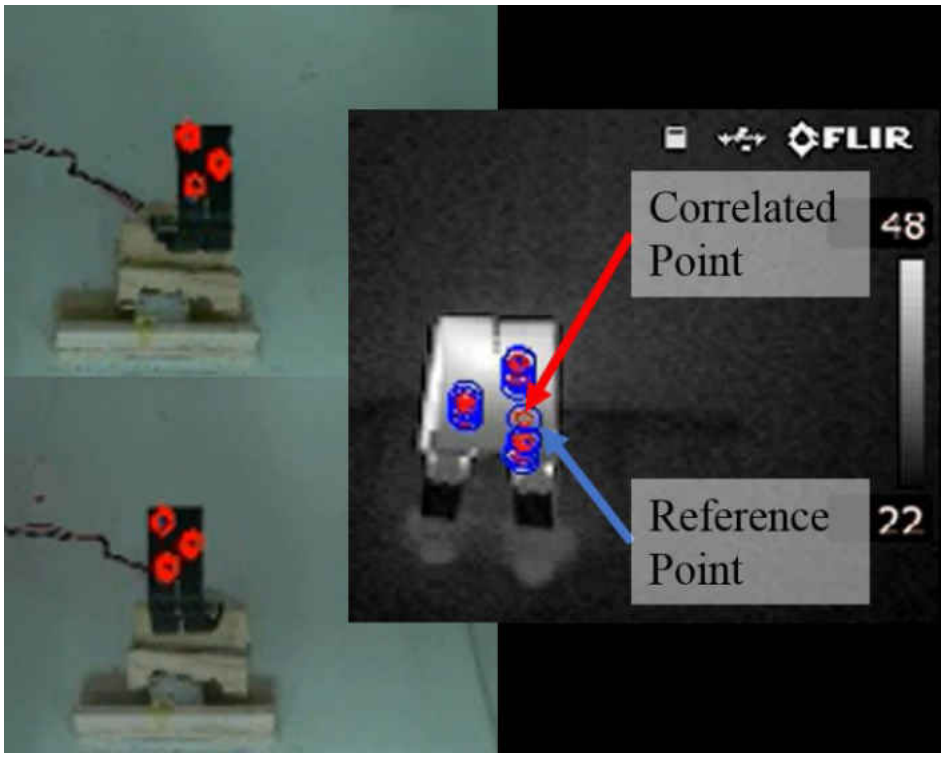

Figure 5.7: Moving structure tracking with correlation[29]

The accuracy of this correlation process is dependent on several factors, including the quality of both the calibration images captured and the accuracy of the calibration process of each individual camera. If there are errors in either of these two steps, they will be propagated though the stereo calibration and result in the correlated result being outside of the desired

tolerances. Another factor affecting the accuracy of the correlation process is the resolution of the cameras used. If the resolution of the camera is too low, the tracking of the points cannot be maintained consistently, but if the resolution is too high latency issues will arise and cause tracking to be lost due to the point of interest leaving the search region before it is detected. Finally, changes in the camera positions will invalidate the transformation matrices used, requiring the cameras to be re-calibrated.

CHAPTER 6

CONCLUSIONS AND FUTURE WORK

A discussion of stereo and thermal camera calibration has been presented with an application of correlating points in 3D space to their respective locations in a thermal image. The benefit of finding these points is it allows for finding surface temperatures at any point of interest which can be tracked with conventional object tracking algorithms for RGB cameras.

This testbed has a field of vision which contains an 8 inch cube but the system could easily be expanded to view larger objects and more cameras could be integrated to retain the surface resolution desired for accurate tracking. Since the testbed is capable of this scaling feature it could have numerous other applications in which accurate spatial temperature measurements are required.

This testbed has further potential in smart materials research as well where actuation is temperature dependent such as with shape memory polymers or shape memory alloys. The ability to monitor the surface temperature of actuating smart materials in real time could lead to more precise actuation control as well as increasing controllability to actuate to more complex geometries. These controllers would require the use of model based robust controllers which would require accurate models to be effective. This testbed is also capable of helping create these models through the identification process developed which provide a

more fundamental understanding of the behavior of the base materials as well as in composite structures which could open up more applications in the future.

6.1 Future Work

In the future, a better model based controller needs to be developed to be able to control the actuation geometry of the shape memory polymer composite structures. The better shape control could open shape memory polymers up to new applications in deployable structures [32][24][25][26], aircraft wing morphing structures [33][27][28] and other unknown applications which present themselves.

LIST OF REFERENCES

[1] Adrien Bak, Samia Bouchafa, and Didier Aubert. Dynamic objects detection through visual odometry and stereo-vision: a study of inaccuracy and improvement sources. *Machine Vision and Applications*, 2014.

[2] Li Hexi and Zhang Juanjuan. 3-d measurement and reconstruction of workpieces in robotic stereovision system. *Applied Mechanics and Materials*, 2014.

[3] Deukhyeon Kim, Jinwook Choi, Hunjae Yoo, Ukil Yang, and Kwanghoon Sohn. Rear obstacle detection system with fisheye stereo camera using hct. *Expert Systems with Applications*, 2015.

[4] Alessandro Verri Trucco. *Introductory techniques for 3-D computer vision*. Prentice Hall, 1998.

[5] Zhengyou Zhang. A flexible new technique for camera calibration. *IEEE Transactions on Pattern Analysis and Machine Intelligence*, 22(11):1330, 2000.

[6] J. Heikkila and O. Silven. A four-step camera calibration procedure with implicit image correction. In *Proc. IEEE Comput. Soc. Conf. Computer Vision and Pattern Recognition (CVPR97)*, 1997.

[7] S. Vidas, R. Lakemond, S. Denman, C. Fookes, S. Sridharan, and T. Wark. A mask-based approach for the geometric calibration of thermal-infrared cameras. *IEEE T Instrum Meas*, 2012.

[8] Y.H. Ng and R. Du. Acquisition of 3d surface temperature distribution of a car body. In *Proc. IEEE Int. Conf. Inf. Acquisition*, 2005.

[9] V. Hilsenstein. Surface reconstruction of water waves using thermographic stereo imaging. In *Proc. Image Vis. Comput*, 2005.

[10] Carol Martnez, Thomas Richardson, Peter Thomas, Jonathan Luke du Bois, and Pascual Campoy. A vision-based strategy for autonomous aerial refueling tasks. *Robotics and Autonomous Systems*, 61(8):876 – 895, 2013.

[11] Adrin Jimnez-Gonzlez, Jose Ramiro Martinez-de Dios, and Anibal Ollero. Testbeds for ubiquitous robotics: A survey. *Robotics and Autonomous Systems*, 61:1487 – 1501, 2013.

[12] WR Wilson, LL Jones, and MA Peck. A multimodule planar air bearing testbed for cubesat-scale spacecraft. *JOURNAL OF DYNAMIC SYSTEMS MEASUREMENT AND CONTROL-TRANSACTIONS OF THE ASME*, 135(4), 2013.

[13] Robert Sivilli. Vision-based testbeds for control system applications. Master's thesis, University of Central Florida, 2012.

[14] C. Liu, H. Qin, and P. T. Mather. Review of progress in shape-memory polymers. *J. Mater. Chem.*, 17:1543–1558, 2007.

[15] Andreas Lendlein, Hongyan Jiang, Oliver Jnger, and Robert Langer. Light-induced shape-memory polymers. *Nature*, 434(7035):879 – 882, 2005.

[16] R. Mohr, K. Kratz, T. Weigel, M. Lucka-Gabor, M. Moneke, and A. Lendlein. Initiation of shape-memory effect by inductive heating of magnetic nanoparticles in thermoplastic polymers. *Proceedings of the National Academy of Sciences of the United States of America*, (10):3540, 2006.

[17] AM Ortega, CM Yakacki, SA Dixon, R Likos, AR Greenberg, and K Gall. Effect of crosslinking and long-term storage on the shape-memory behavior of (meth)acrylate-based shape-memory polymers. *SOFT MATTER*, 8(28):7381 – 7392, 2012.

[18] Wenxin Wang, Dongyan Liu, Yanju Liu, Jinsong Leng, and Debes Bhattacharyya. Electrical actuation properties of reduced graphene oxide paper/epoxy-based shape memory composites. *Composites Science and Technology*, 106:20 – 24, 2015.

[19] A. Lendlein and R.S. Langer. Biodegradable shape memory polymeric sutures, November 6 2012. US Patent 8,303,625.

[20] Christopher Michael Yakacki, Robin Shandas, Craig Lanning, Bryan Rech, Alex Eckstein, and Ken Gall. Unconstrained recovery characterization of shape memory polymer networks for cardiovascular applications. *Biomaterials*, 28:2255 – 2263, 2007.

[21] Joanna Jaworska, Katarzyna Jelonek, Michal Sobota, Janusz Kasperczyk, Piotr Dobrzynski, Monika Musial-Kulik, Anna Smola-Dmochowska, Henryk Janeczek, and Bozena Jarzabek. Shape-memory bioresorbable terpolymer composite with antirestenotic drug. *Journal of Applied Polymer Science*, 132(17), 2015.

[22] YJ Liu, HY Du, LW Liu, and JS Leng. Shape memory polymers and their composites in aerospace applications: a review. *SMART MATERIALS AND STRUCTURES*, 23(2), n.d.

[23] Francis W, Lake M S, Mallick K, Freebury G E, and Maji A. Development and testing of a hinge/actuator incorporating elastic memory composites. In *44th AIAA/ASME/ASCE/AHS/ASC Structures, Structural Dynamics and Materials Conf.*, 2003.

[24] Yang P. *Research on the structure of space deployable antenna based on shape memory polymer composites*. PhD thesis, Harbin Institute of Technology, 2011.

[25] Keller P N, Lake M S, Codell D, Barrett R, Taylor R, and Schultz M R. Development of elastic memory composite stiffeners for a flexible precision reflector. In *47th AIAA/ASME/ASCE/AHS/ASC Structures, Structural Dynamics, and Materials Conf.*, 2006.

[26] Knoll C F Lin J K H and Willey C E. Shape memory rigidizable inflatable (ri) structures for large space systems applications. In *47th AIAA/ASME/ASCE/AHS/ASC Structures, Structural Dynamics and Materials Conf*, 2006.

[27] Weilong Yin, Tao Fu, Jincang Liu, and Jinsong Leng. Structural shape sensing for variable camber wing using fbg sensors. *Proceedings of SPIE*, 2009.

[28] Kai Yu, Weilong Yin, Shouhua Sun, Yanju Liu, and Jinsong Leng. Design and analysis of morphing wing based on smp composite. *Proceedings of SPIE*, 2009.

[29] H. Shen, K. Thompson, A. Mark, Y. Xu, F. Liang, J. Gou, and B. Mabbott. Platform for monitoring and control of electrically actuated shape memory polymer nanocomposite structures. *IEEE/ASME Transactions on Mechatronics*, 2015.

[30] J. Heikkila and O Silven. Camera calibration toolbox for matlab, 1997. `http://www.vision.caltech.edu/bouguetj/calib_doc/`, First accessed 8-30-2013.

[31] H. Shen, A. Mark, K. Thompson, Y. Xu, F. Liang, J. Gou, and B. Mabbott. Thermal modeling and coefficient identification of shape memory polymer nanocomposites structure. *Appl. Phys. Lett.*, 2015.

[32] J. Roh, H. Kim, and J. Bae. Shape memory polymer composites with woven fabric reinforcement for self-deployable booms. *Journal of Intelligent Material Systems & Structures.*, 2014.

[33] I. Kuder, A. Arrieta, W. Raither, and P. Ermanni. Variable stiffness material and structural concepts for morphing applications. *Progress in Aerospace Sciences*, 2013.